Analyst

Cite this: *Analyst*, 2011, **136**, 1496

www.rsc.org/analyst

PAPER

Development of a novel single sensor multiplexed marker assay

Jeffrey T. La Belle,*[a] Ugur Korcan Demirok,[b] Dharmendra R. Patel[c] and Curtiss B. Cook[d]

Received 18th November 2010, Accepted 9th January 2011
DOI: 10.1039/c0an00923g

There is an increasing desire to measure multiple analytes simultaneously for disease management and detection. However, in the case of invasive devices, it would be better to obtain one small sample and immediately be able to detect the analytes rapidly, as in the case of self-monitoring blood glucose, without the need for additional steps, arrays, or reagents. Electrochemical impedance spectroscopy is used to measure the interaction between ultralow levels of analyte and molecular recognition element in a label-free and rapid manner. Gold nanoparticles were attached to antibodies against interleukin-12 and tumor necrosis factor-α, typical inflammatory markers found with near overlapping responses, on an impedance spectroscopy based biosensor. Cross-reactivity and specificity of tuned antibodies were verified using ELISA. Impedance frequency was quantified by concentration gradients of marker against the device. The natural impedance frequency for interleukin-12 (5.00 Hz) was tuned to a lower frequency four Hertz away from one another for better signal processing. This was accomplished without significantly altering the lower limits of detection (<4 pg ml^{-1} and ~60 pg ml^{-1} for interleukin-12 and tumor necrosis factor-α, respectively), no cross-reactivity and specificity as determined by ELISAs. With modeling the nanoscale effects and further development, a larger tuning will be possible for making a better multiplexed sensor. Although interleukin-12 and TNF-α equivalent circuit calculations were modeled here, a sensor with the potential to measure multiple markers at once might offer a solution on the sensor front for simplified management of conditions such as diabetes, where both glucose and hemoglobin A1c values could be obtained.

1. Introduction

The possibility of assaying from a single sensor has long been postulated by researchers and clinicians from various disciplines. In the case of cancers, a variety of markers (ranging from sialyl Lewis, Thomsen-Friedenreich antigen, polysialic acid, among others) have been indicative of cancers ranging from lung, brain, prostate, skin, or colon.[1] Subtle variations in glycosylated proteins have even been noted with changes in the state of colon or breast cancer.[2] Use of multiple markers is not unique to cancer research either. Various markers for cardiovascular diseases were found to better correlate with the early disease detection and management.[3] In relation to diabetes, useful markers that could be measured might include inflammatory, immunological, or metabolic (*e.g.*, glucose, hemoglobin A1c).[4]

There are many technologies that are used to study multiple markers, called microarrays. The technology to detect multiple markers using microarrays ranges from mechanical,[5] optical,[6] thermal,[7] and electrochemical.[8] However, each one of these techniques either requires multiple sensors, wells, platforms, and/or the use of labeling the target of interest. Electrochemical techniques typically require the use of labels, complicated steps, and stripping potentiometry,[9] or the use of arrays.[10]

There are three major types of electrochemical techniques and each has limitations and advantages. In the case of the technology behind most self-monitoring blood glucose (SMBG) devices, that use amperometric mode of operation[11,12] the only means to monitor multiple markers on a single device typically requires the use of labels,[13] which leads to more complex steps and user error. In potentiometric mode, where the current is driven onto the electrode and the potential developed is quantified, labels are also required to perform multiplexing. The last of the three electrochemical techniques is electrochemical impedance spectroscopy (EIS), where an alternating signal is placed on a bias potential while frequencies from Hz to MHz are scanned. In EIS, the ratio of the input to output signal develops the

[a]*The Harrington Bioengineering Program in the School of Biological Health and Systems Engineering and the Biodesign Institute at Arizona State University, 550 East Orange St., Tempe, AZ, 85287-9709, USA. E-mail: JEFFREY.LABELLE@asu.edu; Fax: +1-480-727-7624; Tel: +1-480-727-9061*

[b]*The Harrington Bioengineering Program in the School of Biological Health and Systems Engineering and the Biodesign Institute at Arizona State University, 550 East Orange St., Tempe, AZ, 85287-9709, USA. E-mail: ugur.demirok@asu.edu; Fax: +1-480-727-7624; Tel: +1-480-727-9061*

[c]*Department of Ophthalmology, Mayo Clinic Arizona, 13400 E. Shea Blvd, Scottsdale, AZ, 85259, USA. E-mail: patel.dave@mayo.edu; Fax: +1-480-301-7326; Tel: +1-480-301-7147*

[d]*Department of Medicine, Division of Endocrinology, Mayo Clinic Arizona, 13400 E. Shea Blvd, Scottsdale, AZ, 85259, USA. E-mail: cook.curtiss@mayo.edu; Fax: +1-480-301-8918; Tel: +1-480-301-7091*

impedance (Z, in ohms), and with the change in phase (Φ) between input and output. Thus, the real (Z') and imaginary (Z'') impedances can be calculated using the equations below:

$$Z' = Z \cos(\Phi) \quad (1)$$

$$Z'' = Z \sin(\Phi) \quad (2)$$

Next, a Nyquist graph is plotted, with the real (Z') impedance as the x-axis, against the negative of the imaginary ($-Z''$) impedance and produces a semicircle-like response in the simplest of cases. The highest frequencies on the x-axis start near the origin, and lower frequencies move out onto the curve. At this point, the impedance is governed by the electron transfer resistance, R_{et}. At the maximum imaginary impedance, the frequency is related to the inverse of 2 times π times R_{et} times the double layer capacitance, C_{dl}. Equivalent circuit diagrams can be made to determine a system's behavior at any frequency. Note, that there are many types of material behavior embedded in a Nyquist plot, ranging from constant phase element (CPE), to Warburg, among others, depending upon surface imperfections or diffusion limited systems.

The major advantage of EIS is that it can be performed in a label-free manner, for small molecules, proteins, or whole cell with the target molecules or cells which exhibit a unique frequency upon binding. In the case of breast cancer, the Thompson–Frederick (TF) antigen has long been thought to be a good indicator in the nipple aspirate fluid (NAF). Since the NAF is considered a minimally invasive medium, it was selected for biosensor development for breast cancer screening using label-free EIS.[14] This resulting sensor demonstrated that the sugars on the TF antigen and the molecular recognition elements (MREs), a sugar binding protein (or lectin), exhibited a maximal detection response at 176.00 Hz. Similarly, development of a label-free diagnostic aid for multiple sclerosis using interleukin-12 (IL-12) as a biomarker demonstrated a 5.00 Hz signal.[15] Whole cell biosensors for the determination of bacterial infection, such as *Salmonella typhimurium*, have also been developed with maximal response at frequencies around 10.00 Hz.[16] Recently this multiplexed sensor array design was implemented for various inflammatory markers and the exact nature of the overlapping problem was verified.[17] Five markers, IL-2, IL-10, IL-12, tumor necrosis factor-α (TNF-α), and interferon-γ (IFN-γ) were studied. The results of the study showed that some of these markers were very close to overlapping with 5, 9.77, 17.44, 31.50, and 117.20 Hz for the IL-12, IFN-γ, TNF-α, IL-2, and IL-10 markers, respectively.

Enhancements to EIS have been made over the years, typically in signal amplification, such as the use of colloidal gold, or gold nanoparticles (AuNPs). Some researchers have demonstrated an amplification affect by using AuNPs in EIS[18] where the addition of the AuNP (and a secondary label step) allows for a more sensitive signal to be produced due to an altered electrical effect on the system. But none have demonstrated any unique means to detect multiple targets on a single sensor. Using more than one sensor to achieve multiple marker sensing is one of those means, as with most many electrochemical techniques, and this has been demonstrated with EIS as well.[19] However, in the case of a disease such as diabetes, noncompliance with a single marker sensor is high,[20,21] but this would only increase if the patients had to make multiple measurements for multiple targets daily. Likewise the other hand, it would be almost impossible to differentiate, label-free, five inflammatory markers on a single device (Fig. 1) due to the closeness of their inherent frequency maxima, as these binding or interaction events occur at different albeit close to one another frequencies. Therefore, a more creative solution is required. By use of frequency dependent analysis of an analyte's interaction with the target, we have developed a means to alter or tune the optimum detection frequency of an analyte–MRE pair away from its native state. MREs were prepared and tuned individually, and integrated onto a single sensor by simple mixing during the fabrication step. Upon addition of the sample to the sensor (like current SMBG devices), multiple analytes' concentrations were monitored simultaneously. This allowed the otherwise closely packed frequency spectra of analyte–MRE pairs to drift away from one another, thereby enabling a sensor with multiple MRE elements to relay information about the nature of the target molecules immobilized on the sensor surface. Here we present the proof of principle for the manipulation of the optimum detection frequency of an analyte–MRE pair demonstrating the tuning, retention of specificity and sensitivity thereof.

2. Results and discussion

2.1 Gold nanoparticle–antibody conjugation

Conjugation of the AuNPs to a well established MRE, a monoclonal antibody (mAb), specifically anti-IL-12, was measured by a pronounced Stokes (red) shift in the surface plasmon resonance (SPR) spectra. Unconjugated AuNPs displayed a plasmon maximum at 516 nm (Fig. 2), whereas upon successful conjugation, a red shift of the same to 526 nm was observed.[22–26] Furthermore, FWHM of the conjugated complex resembled that of the bare AuNPs and the spectrum of the former was free of other absorption maxima at higher wavelengths. This indicates that the amount of the unconjugated AuNPs and the aggregates

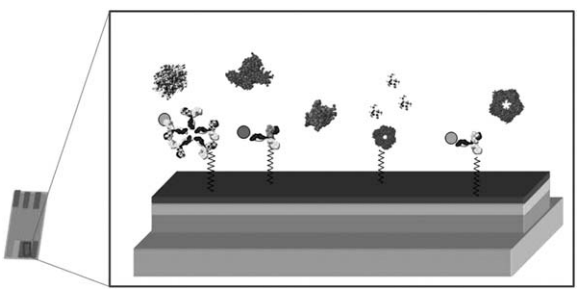

Fig. 1 Conceptual diagram of sensor (left) showing sensor substrate on which Ag/AgCl reference, gold working, gold counter electrodes and electrical leads are fabricated on. Cross-section of sensor surface (right) with 5 possible target systems under study simultaneously. These targets could range from: HbA1c detected by tuned monoclonal antibody, IL-2RA, insulin using its inherent electroactive nature for detection, enzymatic detection of glucose using GDH–FAD, and finally hsCRP detection using tuned monoclonal antibody assay all simultaneously on a single strip sensor.

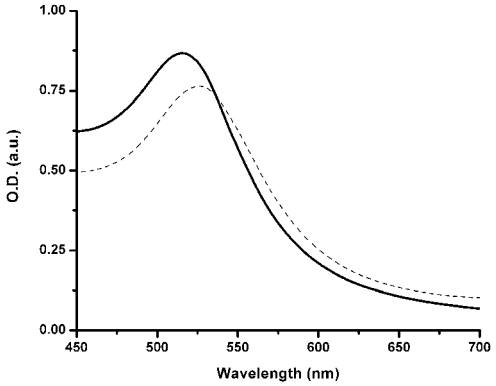

Fig. 2 UV-VIS absorbance spectra showing pre-conjugated spectra for AuNP (solid) with peak at 516 nm and red shifted peak of AuNP conjugated mAb (dashed) with peak at 526 nm.

was insignificant compared to that of the conjugated AuNPs in the final solution.

2.2 Functional verification of gold nanoparticle–antibody conjugates

Successful conjugation is very important to the system but functionality of the conjugates is a must. To determine whether any ill effects occurred during conjugation, such as complete AuNP coverage of the antibody occurred, ELISAs were performed. Firstly, the unconjugated anti-IL-12 was seeded on an ELISA plate and tested against IL-12 target to determine lower limits of detection (LLD) and responsivity as measured by the slope of the curve. The unconjugated anti-IL-12 bound IL-12 with an LLD of 3.9 pg mL^{-1} and a responsivity of 7.3×10^{-4} ($n = 3$, $R^2 = 0.999$). However, the AuNP conjugated anti-IL-12, when tested against a concentration gradient, exhibited some decrease in LLD = 60 pg mL^{-1} and responsivity = 3.6×10^{-5} ($n = 3$, $R^2 = 0.999$). To test against specificity, another protein, namely TNF-a, was run in the anti-IL-12 ELISA with minimal signal detection (Fig. 3).

The results from the TNF-α ELISA were similar in trends. The unconjugated anti-TNF-α : TNF-α results had an LLD of 3.4 pg mL^{-1} and responsivity = 4.3×10^{-4} ($n = 3$, $R^2 = 0.999$) and when conjugated, the system's LLD went to 109 pg mL^{-1} with responsivity = 4.3×10^{-5} ($n = 3$, $R^2 = 0.999$). Again, there was little to no cross-reactivity when presented with the other marker, IL-12 in this case (Fig. 4). This loss of the LLD and responsivity

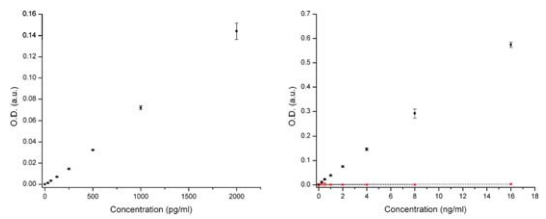

Fig. 3 ELISA verification of AuNP conjugated mAb functionality with "untuned" mAb function against IL-12 (left) compared to "tuned" conjugate (right) against IL-12 (sloping data) and against TNF-a (flat response) showing high specificity remains for IL-12 and little to no cross-reactivity to TNF-a.

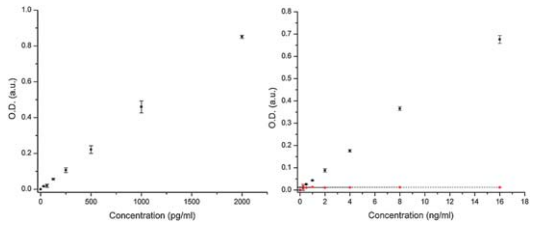

Fig. 4 ELISA verification of AuNP conjugated mAb functionality with "untuned" mAb function against TNF-a (left) compared to "tuned" conjugate (right) against TNF-a (sloping data) and against IL-12 (flat response) showing high specificity remains for TNF-α and little to no cross-reactivity to IL-12.

is an expected result of the conjugation as some of the binding sites on the complexed antibody are used to interact with the surface atoms of the AuNP.

2.3 Tuning electrochemical impedance spectroscopy proof of principle

The initial testing performed included a comparison between two sets of sensors ($n = 4$ total) with two sensors with unconjugated anti-IL-12 immobilized compared to the sensors Nyquist prior to immobilization showing little or slight change in impedance indicating successful immobilization but no altered or adjusted impedance. However, once the immobilization of an AuNP conjugated anti-IL-12 sensor was run, the Nyquist exhibited a marked change in impedance as compared to the reading prior to immobilization (Fig. 5) indicating a significant change in impedance has occurred.

To determine the exact nature of this change, and to see if a successful tuning occurred, a concentration gradient of IL-12 was run against the unconjugated and conjugated sensors. When the concentration gradient was run against the unconjugated antibody sensor, a typical 5.00 Hz signal was seen. However, in the case of the conjugated (or tuned), the maximal response was detected at 1 Hz, 4.00 Hz away from the typical response. Verifying that the 5.00 Hz signal is no longer an optimal frequency on this "tuned" sensor shows that even such a small change in signal is measurable over 4 log orders of concentration (Fig. 6). This shift of 4.00 Hz was performed using a 10 nm AuNP. However, when a smaller particle is used, the impedance of the conjugate system displays astarker adjustment due to further quantization

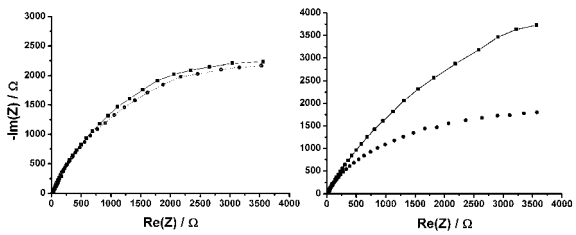

Fig. 5 Left: Nyquist responses (solid) with immobilized unconjugated antibodies and (dashed) bare electrodes (with no linker or antibody). Nyquist responses (right) for electrodes with conjugated antibodies immobilized on them (solid) and with no AuNPs conjugated on them (dashed). Note: all sensors were run "bare" prior to antibody or antibody–AuNP conjugates were attached to them.

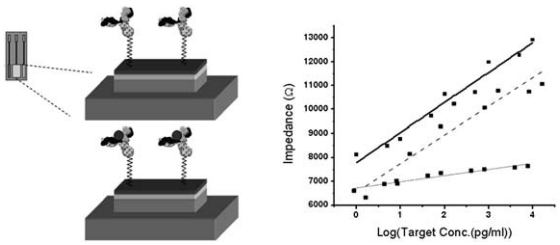

Fig. 6 Schematics for (left) "untuned" (upper) and AuNP "tuned" (lower) mAb with results demonstrating feasibility (right) with "untuned" anti-IL-12 : IL-12 binding showing typical 5 Hz optimal response (solid) to "tuned" response now shifted to 1 Hz (dashed) as well as verification of reduced 5 Hz response for the "tuned" system back at 5 Hz (dotted line).

and a higher degree of signal shifting is possible. In the case of two targets being close to one another, one type of tuning element could shift the lower frequency even lower while the other tuning element could shift the higher one higher, thereby optimizing these two to be the furthest away from one another as possible. As most biomarkers have demonstrated frequencies associated with them at or below 1 kHz, this method of tuning will readily allow for at least five biomarkers to be tuned significantly apart in this region.

3. Experimental

3.1 Gold nanoparticle–antibody conjugation

The AuNPs used in this study were prepared according to a method described earlier in the literature.[22] Basically commercial AuNPs (Sigma-Aldrich, St Louis, MO) were made by % composition from stocks of 5×10^{13}, 5.7×10^{12} and 7×10^{11} for 5, 10 and 20 nm respectively. By this method, AuNPs of 2–20 nm in diameter were prepared. For 5 nm particles, 1 mL of 1% (w/v) $HAuCl_4$ is mixed with 79 mL of deionized (DI) water and heated to 60 °C. Meanwhile, a reducing mixture of 4 mL of 1% (w/v) trisodium citrate, 5 mL of 1% tannic acid and 5 mL of 2.5 mM K_2CO_3 and 5 mL of DI water is brought to 60 °C and added to the gold solution with stirring. Upon observation of the red color, the resulting solution is boiled for 10 min. For larger particles, lower amounts of tannic acid and potassium carbonate were used in equal amounts (down to 0.01 mL for 20 nm particles) while keeping the total reducing solution volume at 20 mL. The final solution containing the particles was cooled to room temperature and the intensity of UV-VIS absorption, SpectraMax M5 Photospectrometer, Molecular Devices, Sunnyvale, CA at 520 nm, was adjusted to 1 AU by centrifugation before use.

Antibodies and antigens in lyophilized form were purchased from R&D Systems, Minnesota, MN and were reconstituted in phosphate buffered saline (PBS) which was purchased in tablet form from CalBioChem, La Jolla, CA, and was dissolved in DI water to yield a working solution of 140 mM NaCl, 10 mM phosphate buffer and 3 mM KCl, pH 7.4 at 25 °C.

The conjugation of the antibodies with AuNPs was done according to the following procedures. The minimum amount of antibody required to stabilize the AuNPs in a given solution was determined by mixing a series of concentrations of the protein (10–100 ug mL^{-1}, 1 mL) with a millilitre of gold solution and incubation for 5 min. After 5 min, 0.5 mL of 10% (w/v) NaCl was added and the protein concentration at which the gold solution changes the color to blue from red was deemed as the minimum concentration required amount for stabilization. Up to 25% excess protein was used in addition to the minimum concentration determined to ensure a higher degree of conjugate stabilization. The AuNPs were then incubated at room temperature for 20 min after bringing the pH of the colloidal suspension to pH 8–9 with K_2CO_3, which is close to the isoelectric point of most immunoglobulin G (IgG) molecules. The resulting solution was transferred into a Beckman Quick-Seal tube and centrifuged in a Beckman-Coulter Optima L-100 XP Ultracentrifuge at 50 000*g* for 20 nm, 70 000*g* for 10 nm, and 90 000*g* for 5 nm AuNP conjugated antibodies at 4 °C for 1 h to separate unconjugated antibody from the gold–antibody complexes. Dark red colored pellet obtained by centrifugation was then reconstituted in 10 mM PBS. The conjugates were consumed immediately.

Structural assembly of the conjugates was determined by UV-VIS spectroscopy. Spectra were collected prior to and post-conjugation from 450–700 nm from a 1 mL sample using a Shimadzu BioSpec-mini spectrometer after a background of pure buffer was subtracted.

3.2 Functional verification of gold nanoparticle–antibody conjugates

To verify the functional assembly still displayed the same sensitivity and specificity as before, Enzyme Linked Immunosorbent Assays (ELISAs) were performed. All reagents were purchased from R&D Systems, Minnesota, MN, and four plates were developed according to the following protocols. 100 μL, 10 μg mL^{-1} of the appropriate capture antibody/conjugate solution (in PBS) was placed into the wells of a clear polystyrene microplate and the plate was sealed and incubated overnight at 4 °C. The wells were washed with ~400 μL wash buffer (0.05% Tween 20 in PBS) 3 times before blocking the plates with 1% Bovine Serum Albumin in 10 mM PBS, pH 7.4, for 2 h. Following the washing step, 100 μL of the sample antigen (2 ng mL^{-1} in PBS) was added to each well and the plate was gently tapped to ensure proper mixing before the plate was sealed and incubated at 25 °C for 2 h. 100 μL of the biotinylated detection antibody (100 ng mL^{-1} for IL-12 and 200 ng mL^{-1} for TNF-α in PBS) was added to the wells, which were incubated for 2 h at 25 °C before the addition of 100 μL streptavidin–horse radish peroxidase (1/200 dilution factor) for a duration of 20 min at 25 °C. Finally, 100 μL aliquots of the substrate solution were added and the plate was sealed and covered with aluminium foil for 30 min before stopping the reaction with 50 μL stop solution. After thorough mixing, the optical intensity at 450 nm was determined using a Molecular Devices, Silicon Valley, CA, SpectraMax M5 Plate Reader within 30 min. The absorption due to bare plates at 540 and 570 nm was subtracted using the built-in wavelength correction of the instrument.

3.3 Tuning electrochemical impedance spectroscopy proof of principle

Gold disc electrodes (2 mm diameter) purchased from CH Instruments, Inc., Austin, TX were used throughout this study.

Gold electrode was polished for 2 min with 1, 0.3 and 0.05 μm Al_2O_3 powder and was sonicated for 5 min in acetone, ethanol and DI water to remove alumina from the surface. Upon washing the electrode with copious amounts of DI water, cyclic voltammetry (CV) was performed on the bare gold electrode using a three electrode system (Au working electrode, Pt counter electrode and Ag/AgCl reference electrode) in a solution of 5 mM $[Fe(CN)_6]^{3-}/[Fe(CN)_6]^{4-}$, 0.1 M KCl and 10 mM PBS (pH = 7.4) to obtain the formal potential of the system using standard Ag/AgCl reference electrode (~250 mV depending upon electrode used). Impedance measurements were taken subsequently from the electrode at the former potential obtained from CV at a frequency range of 0.10 Hz to 10^5 Hz, with amplitude of 5 mV. All electrochemical measurements were done with a CHI660C analyzer (CH Instruments Inc., Austin Texas, USA).

Immobilization of the anti-IL-12 antibodies onto the sensor surfaces was performed as previously reported.[23] Briefly, self-assembling layer of 16-mercaptohexadecanoic acid (16-MHDA) was formed on the previously cleaned gold electrode though thiol linkages. The electrodes were kept in MHDA solutions having a concentration of 1 mM to 25 mM (in absolute ethanol) for a period varying between 1 and 12 h at room temperature. Most electrodes were immersed in 1 mM MHDA for 1 h at RT.

Carboxylate groups of MHDA were converted to succinimidyl esters by immersing the electrode in an aqueous solution of 40 mM 1-ethyl-3-(3-dimethylaminopropyl) carbodiimide (EDC) in the presence of 10 mM water soluble sulfo-derivative of *N*-hydroxysuccinimide (NHS) for 1 h. After decanting the EDC–NHS and washing the sensor with DI water, the antibody (anti-IL-12 or anti-TNF-α) was then immobilized on the activated sensor surface by immersion into a 10 μg mL^{-1} solution (in PBS) of the desired antibody overnight at 4 °C. The sensor was washed with PBS following immobilization and blocked by ethanolamine using an aqueous solution of 1% (w/v) for 30 min against non-specific binding, prior to antigen exposure at varying concentrations.

Electrochemical impedance spectroscopy was performed using a CHI660C Impedance Analyzer, gold disk working, platinum wire counter, and silver–silver chloride reference electrodes from 100 kHz to 0.10 Hz sweeps using a 250 mV DC offset and 5 mV AC potential. Initial testing was performed using bare gold working electrode and immobilized unconjugated and AuNP conjugated anti-IL-12 immobilized electrodes with 100 μL of 5 mM ferricyanide–ferrocyanide redox probe in 1× PBS at pH 7.4. Concentration gradients of IL-12 were then made from 0 (buffer alone) to 10 000 pg mL^{-1} of target protein. Frequency analysis was used to show impedance at characteristic frequency for binding and plotted against concentration.

4. Conclusions

In this paper, we demonstrated a tuning of the EIS frequency element for the potential of multiplexing multiple markers onto a single sensor. By use of AuNPs conjugated to the MRE, we have shown differential tuning using 5, 10, and 20 nm diameter sizes of AuNPs. By conjugation of the NP to the MRE rather than the target, timely and complicated labeling (of the target) steps were avoided. With this principle, extension of the tuning to 10's to 100's of Hz should be made possible by better selection of alternative sizes, materials, and perhaps particle to MRE spacing. Currently, a model of the nanoscale effects is being developed that will incorporate these factors into a single function of particle size and frequency shift, which in turn could be used to help explain the current observations and provide further insight on how to increase the tuning response.

The technology described here may have important uses for the management of chronic diseases such as diabetes. Specific markers for diabetes could be studied using EIS to determine maximal response frequencies, and designing the tuning required. As such, various metabolic, inflammatory and immunological markers relevant to diabetes such as glucose, insulin, CRP, IL-2RA, and HbA1c[27,28] could be incorporated into a single test strip, which in turn could bring the technology one step closer to providing a new paradigm for more effective care.

Abbreviations

SMBG	self-monitoring of blood glucose
HbA1c	glycosylated hemoglobin
CRP	C-reactive protein
IL-2RA	interleukin-2 receptor A
EIS	electrochemical impedance spectroscopy
Z	impedance
Φ	phase
Z'	real impedance
Z''	imaginary impedance
R_s	solution resistance
R_{et}	electron transfer resistance
C_{dl}	double layer capacitance
CPE	constant phase element
MRE	molecular recognition element
NAF	nipple aspirate fluid
TF	Thompson–Frederick antigen
IL-12	interleukin-12
AuNPs	gold nanoparticles
TNF-α	tumor necrosis factor-α
IFN-γ	interferon-γ
DI	Deionized
PBS	phosphate buffered saline
IgG	immunoglobulin G
ELISA	Enzyme Linked Immunosorbent Assay
16-MHDA	16-mercaptohexadecanoic acid
EDC	1-ethyl-3-(3-dimethylaminopropyl) carbodiimide
NHS	sulfo-derivative of *N*-hydroxysuccinimide
FWHM	full width at half maximum
CV	cyclic voltammetry
mAb	monoclonal antibody
LLD	lower limits of detection
UV-VIS	ultraviolet-visible

Acknowledgements

The authors graciously thank the Biodesign Institute for support for this project.

References

1 D. H. Dube and C. R. Bertozzi, *Nat. Rev. Drug Discovery*, 2005, **4**, 477–488.
2 I. Brockhausen, *EMBO Rep.*, 2006, **7**, 599–604.
3 R. S. Vasan, *Circulation*, 2006, **113**, 2335–2362.
4 J. A. Kolberg, T. Jorgensen, R. W. Gerwien, S. Hamren, M. P. McKenna, E. Moler, M. W. Rowe, M. S. Urdea, X. M. Xu, T. Hansen, O. Pederson and K. Borch-Johnsen, *Diabetes Care*, 2009, **32**, 1207–1212.
5 B. Zhang, X. Zhang, H.-h. Yan, S.-j. Xu, D.-h. Tang and W.-l. Fu, *Biosens. Bioelectron.*, 2007, **23**, 19–25.
6 J. N. Anker, W. P. Hall, O. Lyandres, N. C. Shah, J. Zhao and R. P. Van Duyne, *Nat. Mater.*, 2008, **7**, 442–453.
7 T. Maskow, J. Lerchner, M. Peitzsch, H. Harms and G. Wolf, *J. Biotechnol.*, 2006, **122**, 431–442.
8 P. S. Petrou, I. Moser and G. Jobst, *Biosens. Bioelectron.*, 2002, **17**, 859–865.
9 L. Chen, Z. Qi, R. Chen and S. Liu, *Clin. Chim. Acta*, 2010, **411**, 1969–1975.
10 Y. Pan, G. A. Sonn, M. L. Y. Sin, K. E. Mach, M.-C. Shih, V. Gau, P. K. Wong and J. C. Liao, *Biosens. Bioelectron.*, 2010, **26**, 649–654.
11 M. Rosu and A. Schumpe, *Chem. Eng. Sci.*, 2009, **65**, 220–225.
12 J. D. Newman and A. P. F. Turner, *Biosens Bioelectron.*, 2005, **20**, 2435–2453.
13 Z. Dai, A.-N. Kawde, Y. Xiang, J. T. La Belle, J. Gerlach, V. P. Bhavanandan, L. Joshi and J. Wang, *J. Am. Chem. Soc.*, 2006, **128**, 10018–10019.
14 J. T. La Belle, J. Q. Gerlach, S. Svarovsky and L. Joshi, *Anal. Chem.*, 2007, **79**, 6959–6964.
15 K. Bhavsar, A. Fairchild, E. Alonas, D. K. Bishop, J. T. La Belle, J. Sweeney, T. L. Alford and L. Joshi, *Biosens. Bioelectron.*, 2009, **25**, 506–509.
16 J. T. La Belle, M. Shah, J. Reed, V. Nandakumar, T. L. Alford, J. W. Wilson, C. A. Nickerson and L. Joshi, *Electroanalysis*, 2009, **21**, 2267–2271.
17 A. B. Fairchild, K. McAferty, U. K. Demirok and J. T. La Belle, *IEEE-ICME*, 2009, Apr, 1–5, DOI: 10.1109/ICCME.2009.4906678.
18 X. Yu, R. Lv, Z. Ma, Z. Liu, Y. Hao, Q. Li and D. Xu, *Analyst*, 2006, **131**, 745–750.
19 H. Chen, J. H. Jiang, Y. Huang, T. Deng, J.-S. Li, G.-L. Shen and R.-Q. Yu, *Sens. Actuators, B*, 2006, **117**, 211–218.
20 S. L. Tunis and M. E. Minshall, *Curr. Med. Res. Opin.*, 2010, **26**, 151–162.
21 L. Heinemann, *J. Diabetes Sci. Technol.*, 2008, **2**, 919–921.
22 J. W. Slot and H. J. A. Geuze, *Eur. J. Cell Biol.*, 1985, **38**, 87–93.
23 J. T. La Belle, K. Bhavsar, S. Svarovsky, P. Zhang, V. Bhavanandan, J. Sweeney, T. Alford, J. Wang and L. Joshi, *Biosens. Bioelectron.*, 2007, **23**, 428–431.
24 V. Shakila and K. Pandian, *J. Solid State Electrochem.*, 2007, **11**, 296–302.
25 J. Swift, A. Butts, J. Cheung-Lau, V. Yerubandi and I. J. Mochowski, *Langmuir*, 2009, **25**, 5219–5225.
26 Y. Liu, M. K. Shipton, J. Ryan, E. D. Kaufman, S. Franzen and D. L. Feldheim, *Anal. Chem.*, 2007, **79**, 2221–2229.
27 J. A. Kolberg, T. Jorgenson, R. W. Gerwien, S. Hamren, M. P. McKenna, E. Moler, M. W. Rowe, M. S. Urdea, X. M. Xu, T. Hansen, O. Pedersen and K. Borch-Johnsen, *Diabetes Care*, 2009, **32**, 1207–1212.
28 M. E. Williams, E. Lacson, Jr, M. Teng, N. Ofsthun and J. M. Lazarus, *Kidney Int.*, 2006, **70**, 1503–1509.